RESEARCH ARTICLE | NOVEMBER 24 2025

Simulating plastic ice VII with the data-driven many-body MB-pol potential

Special Collection: Carlos Vega Festschrift

Francesco Guidarelli Mattioli ; Xuanyu Zhu ; Francesco Paesani ; Livia E. Bove ; John Russo ; Francesco Sciortino

J. Chem. Phys. 163, 204501 (2025)
https://doi.org/10.1063/5.0296428
CHORUS

The Journal of Chemical Physics ARTICLE pubs.aip.org/aip/jcp

Simulating plastic ice VII with the data-driven many-body MB-pol potential

Cite as: J. Chem. Phys. 163, 204501 (2025); doi: 10.1063/5.0296428
Submitted: 13 August 2025 • Accepted: 4 November 2025 •
Published Online: 24 November 2025

Francesco Guidarelli Mattioli,[1] Xuanyu Zhu,[2] Francesco Paesani,[2] Livia E. Bove,[1,3] John Russo,[4] and Francesco Sciortino[4,a)]

AFFILIATIONS

[1] Department of Physics, Sapienza University of Rome, Piazzale Aldo Moro 5, I-00185 Roma, Italy
[2] Department of Chemistry and Biochemistry, University of California, San Diego, La Jolla, California 92093, USA
[3] Sorbonne Université, UMR CNRS 7590, Institut de Minéralogie, de Physique des Matériaux et de Cosmochimie (IMPMC), 5 Place Jussieu, 75005 Paris, France
[4] Physics Department, Sapienza University of Rome, Piazzale Aldo Moro 5, I-00185 Roma, Italy

Note: This paper is part of the Special Topic, Carlos Vega Festschrift.
[a)] **Author to whom correspondence should be addressed:** francesco.sciortino@uniroma1.it

ABSTRACT

Computational studies using effective potentials that treat water as a rigid molecule were the first to predict the existence of a plastic phase of ice VII. Fifteen years later, this prediction was confirmed experimentally: in the plastic phase, water molecules retain the translational order of the body-centered cubic lattice while undergoing jump-like rotational motion typical of the liquid. Here, we show that this plastic phase also emerges in simulations employing the data-driven many-body MB-pol potential. The phase appears at high pressure, sandwiched between the liquid and ice VII phases. Our results confirm the first-order nature of both the ice VII–plastic and plastic–liquid transitions. Moreover, we find that ice VII exhibits rotational motion of hydrogen atoms on the nanosecond timescale near the melting line, although this motion is qualitatively distinct from that observed in the plastic phase. These results support the existence of the plastic phase beyond rigid-molecule models and provide new insight into the rotational dynamics of ice under extreme conditions.

I. INTRODUCTION

Water continues to challenge our understanding of condensed matter with its rich and often counterintuitive phase behavior,[1,2] both in the liquid and in the crystal regions.[3] Over the past decades, the exploration of water's phase diagram under extreme thermodynamic conditions has revealed a multitude of crystalline and amorphous forms, each characterized by distinct structural, dynamical, and thermodynamic features. Among these, ice VII[4]—a high-pressure polymorph of ice stable above 2 GPa—occupies a central place due to its relevance in planetary interiors, particularly for large icy moons and giant icy planets.[5–8] Structurally, ice VII consists of a body-centered cubic lattice of oxygen atoms, with each water molecule hydrogen-bonded to four neighbors in a disordered hydrogen configuration that distinguishes it from ordered counterparts such as ice VIII. The positions of the oxygens can be visualized as two interpenetrating diamond cubic lattices.[9]

Computational studies based on classical rigid water models—from the group of Tanaka[10–12] and of Vega[13,14]—have been first in predicting the possible emergence of a plastic phase of ice VII, in which water molecules retain the translational order of the crystalline lattice while undergoing quasi-free rotational motion. In this phase, the hydrogen-bond network is topologically distinct from ice VII.[15] Free-energy calculations showed the thermodynamic stability of the plastic phase above a model-dependent triple point (among ice VII, plastic, and liquid phases) located below 10 GPa. Further studies examined the structure and dynamics of water plastic crystals,[16] as well as their dielectric properties.[17] The potential existence of a water bcc plastic ice has also recently been supported by *ab initio*[18] and reactive force fields.[19]

A different prediction was later proposed in a simulation study[20] based on a deep neural network potential trained according to the DeePMD framework[21] on electronic structure data calculated for water and various ice polymorphs over a range of temperatures

and densities using the SCAN functional.[22] This study did not find evidence of a plastic phase, suggesting instead that above 10 GPa ice VII transforms into ice VII′ and VII″, ionic phases characterized by partial molecular dissociation and breaking of the ice rules. It should be noted that the SCAN functional exhibits functional-driven and density-driven errors,[23,24] which have been shown to limit the SCAN accuracy in reproducing the phase behavior of water.[20] A plastic phase was also not found in simulations performed with a neural network potential.[25] Experimental dielectric measurements have also suggested that, at 10 GPa, hydrogen atoms undergo a hopping translational dominant dynamics.[26]

Until recently, the plastic phase had eluded experimental confirmation, largely due to the challenges in probing molecular orientations under the required high-pressure and high-temperature conditions. However, recent experimental observations[27] based on quasi-elastic neutron scattering[28] (which probe the dynamics of hydrogen atoms) have now confirmed the existence of a plastic state in the 5–6 GPa and 480–550 K region, in which molecules exhibit jump rotational dynamics on the picosecond time scale. While providing direct evidence of a plastic phase, the experimental study focused on dynamical observables and, thus, could not provide conclusive results on the thermodynamic nature of the transition, e.g., whether it is continuous or discontinuous.

Here, we revisit the problem of the existence of a thermodynamically stable plastic phase using the data-driven many-body MB-pol potential. MB-pol accurately predicts the properties of liquid water across a wide range of thermodynamic conditions.[29,30] Below 1 GPa, it can reproduce the stability field of all known crystalline forms of water.[31] It has also been shown that MB-pol predicts a liquid–liquid critical point around 200 K and 1200 bar,[32] in agreement with extrapolations based on experimental data for the volume of liquid water measured over a wide pressure–temperature range.[33] The MB-pol potential represents a significant advancement in the modeling of water, being based on high-level electronic structure calculations, which do not suffer from the approximations intrinsic in the density functional theory, and its many-body expansion of the energy is rigorously derived.[34–36] By construction, MB-pol neglects molecular dissociation, limiting its applicability to non-ionic phases. Unlike the previously studied TIP5P[37] and TIP4P-2005[38] models, MB-pol retains the flexibility of water molecules. Recently, MB-pol has been reformulated using permutationally invariant Fourier series (PIFSs) as its functional basis.[39] This new formulation, referred to as MB-pol(PIFS), improves the numerical robustness of the potential energy function and mitigates the occurrence of catastrophically negative energies (so-called "holes"), which may become relevant at high pressures.

In this study, we used MB-pol(PIFS) to perform simulations over a wide range of temperatures and pressures, encompassing the conditions under which the transition from fully hydrogen-disordered ice VII to the plastic phase has been observed experimentally. We focus on characterizing the equation of state and the dynamics in the different phases and evaluating the pressure–temperature coexistence lines between liquid, plastic, and ice VII phases. We find that the MB-pol(PIFS) predicts the existence of a plastic phase with a density intermediate between that of the crystal and the liquid, supporting the first-order nature of the ice VII–plastic transition. We observe that ice VII also exhibits rotational dynamics near its melting line, but with important differences compared to the plastic phase. First, rotational motion in ice VII occurs on the nanosecond timescale, significantly slower than the picosecond timescale observed in the plastic phase, and it is limited to 180° rotations around the dipole vector. Second, in ice VII, rotations are activated events between the stable configurations in which each molecule is always bonded to the same diamond-cubic lattice. In contrast, the plastic phase features stable configurations in which molecules can transiently form hydrogen bonds across both interpenetrating sublattices. Finally, we discuss the accuracy of the current version of the MB-pol(PIFS) potential and examine the implications of the commonly accepted definition of "chemical accuracy" (e.g., 1 kcal/mol), particularly in cases where relevant free-energy differences are on the order of a few tenths of a kcal/mol. We also outline possible future improvements of MB-pol(PIFS).

II. METHODS

A. The MB-pol(PIFS/A1) potential

In this work, we use the MB-pol(PIFS/A1) potential, referring to the PEF/A1 version presented in the Supporting Information of Ref. 39. MB-pol(PIFS/A1) is a variant of the data-driven many-body MB-pol potential.[34–36] This potential is based on machine-learned short-range n-body terms (with $n \leq 3$) learned from *ab initio* data calculated at the coupled cluster level of theory, which are integrated with a physics-based term representing two-body dispersion and many-body electrostatics at all molecular separations. MB-pol(PIFS/A1) improves upon MB-pol by ensuring stability at high pressures while maintaining the same robustness under ambient conditions.[39] For a detailed description of MB-pol(PIFS/A1) and an assessment of its accuracy, the interested reader is referred to Ref. 39.

B. Computational details

We investigated the high-pressure phase diagram of water by performing MD simulations in the isothermal–isobaric (*NPT*: constant number of particles, pressure, and temperature) ensemble at different pressures and temperatures using the LAMMPS package[40] patched with MBX.[41,42] We started by generating an ice VII crystal configuration of 864 water molecules with GenIce[9] (replicating the unit box by 6-3-3 factors, producing a box of approximately side 4-2-2 nm). We simulated for at least 40 ps with a time step of 0.2 fs, running with the openMP version of MBX on 40 cores. We observed the spontaneous melting of ice VII to liquid water at 5.5 and 7 GPa by increasing the temperature. At higher pressures (9 and 11 GPa), we first observed the spontaneous transition from ice VII to the plastic phase, followed by melting of the plastic phase into the liquid at higher temperatures. We performed direct coexistence simulations for liquid–ice VII and liquid–plastic ice phase in the *NPT* ensemble to unveil the phase diagram. To prepare the coexistence box, we first equilibrated the liquid and ice phases using *NPT* simulations (each phase being composed of 864 water molecules) and calculated the corresponding equilibrium densities. We then scaled the liquid box such as the zy side perfectly overlaps with the ice zy side and scaled the z axis of the liquid box to preserve the correct liquid density. The interface between the liquid and ice was further equilibrated with a Nosé–Hoover barostat applied to the x axis, keeping the number of ice molecules fixed. Throughout these simulations, we monitored ice growth by calculating a local

bond-order parameter.[43] We also computed the coexistence line by integrating the Gibbs–Duhem equation (following Ref. 44) with a pressure step of 0.25 GPa and using the direct coexistence pressure and temperature values as initial conditions.

C. Assessment of MB-pol(PIFS/A1)

Although MB-pol(PIFS/A1) preserves, and in some cases improves, the accuracy of MB-pol for gas-phase clusters and liquid water at ambient pressure, its performance for high-pressure phases of water has not been fully assessed. The simulations presented in this work reveal discrepancies with experimental observations, which are discussed in this section. One notable issue is the MB-pol(PIFS/A1)'s tendency to favor proton ordering at elevated pressures. As a result, extended classical MD simulations, particularly those near the melting temperature, often evolve from the disordered ice VII phase toward the fully proton-ordered ice VIII phase. This behavior indicates that, under such conditions, classical MD simulations with MB-pol(PIFS/A1) predict ice VIII to be the thermodynamically stable phase.

Our analysis suggests that this discrepancy likely arises from n-body contributions with $n > 3$, which are not quantitatively reproduced by many-body polarization. Specifically, like MB-pol, the MB-pol(PIFS/A1) potential includes machine-learned corrections up to the three-body term, while four-body and higher-order contributions are approximated using a classical polarizable model. We found that, despite remaining within "chemical accuracy," the errors in the four-body term become comparable to the relevant free-energy differences at high pressure, leading to a slight overestimation of both the lattice energy (by ~0.5 kcal/mol) and the unit cell volume of ice VII. At high pressure, the Gibbs free-energy difference between ice VII and ice VIII $[\Delta G(P,T) = \Delta E + P\Delta V - T\Delta S]$ is highly sensitive to small variations (below ~0.5 kcal/mol) in all three contributing terms, due to the elevated pressure and the relatively small entropic differences between the two phases. As a result, even deviations significantly smaller than "chemical accuracy" in MB-pol(PIFS/A1)'s predictions can introduce noticeable uncertainty in the computed location of the phase coexistence line. These observations suggest that incorporating an explicit four-body PIFS correction into MB-pol(PIFS/A1) could be a valuable direction for future development. In addition, it may be worth investigating nuclear quantum effects, as their impact on enthalpy (and thus volume) and entropy could remain non-negligible due to the sensitivity of free-energy differences, as previously observed in water clusters.[45–49] Numerical analyses of the free-energy differences associated with the ice VII–ice VIII equilibrium are provided in the supplementary material.

Nevertheless, for the purposes of this study, we have focused exclusively on the metastable, disordered ice VII phase. Owing to its long lifetime on the simulation timescales considered here (nanoseconds), ice VII remains well-defined and enables a meaningful analysis of its phase behavior. We explicitly verified that all simulations, both bulk ice VII and direct coexistence setups with the liquid, maintain proton disorder throughout their duration, confirming that the observed transitions are not artifacts of proton ordering. It should also be noted that we encountered numerical instabilities in some MD simulations. These are limited to high-density plastic and liquid phases, and typically occur after tens of ps in half of the simulated trajectories, whereas other runs went beyond 100 ps with no crashes. These instabilities suggest that MB-pol(PIFS/A1) occasionally predicts dissociation events, which violate the assumptions underlying the many-body framework on which the model is based. It remains unclear whether these dissociation events reflect physical phenomena or stem from numerical artifacts. Further investigation is needed to assess their sensitivity to possible sources of inaccuracy, including the omission of four-body energy corrections, nuclear quantum effects, errors introduced by the numerical fitting in MB-pol(PIFS/A1), and possible intrinsic inaccuracies in the coupled cluster n-body energies that are used for training.

III. RESULTS

A. Thermodynamic differences

Figure 1(a) shows the temperature dependence of the density at four different pressures as calculated from *NPT* simulations. For each pressure, the results are shown for simulations starting from an initial configuration in the ice VII phase, from a liquid phase configuration and (when existing) from a plastic configuration. At pressures of ~9 GPa and above, a temperature of ~600 K, ice VII transformed spontaneously [see Fig. 1(b)] into a plastic phase, which remained stable on the timescale of our simulations. As for the TIP4P/2005 model, the transition was accompanied by a finite change in density (~4% change with respect to the density of ice VII), supporting its first-order nature. At higher temperatures, the plastic phase spontaneously transformed into a liquid phase. A similar phenomenon was observed at 11 GPa, with again a discontinuous change in density at the two transitions. *NPT* simulations, which were initiated in the plastic phase, remained in the plastic phase in a finite temperature interval during the probed simulation time scale.

Bulk simulations with periodic boundary conditions tend to overestimate the stability range of any thermodynamic phase, as they lack interfaces, heterogeneous nucleation sites, and are affected by intrinsic barriers to homogeneous nucleation. Consequently, although the abrupt density jump shown in Fig. 1 suggests the existence of an intermediate phase between ice VII and the liquid, the temperature at which this change occurs is not thermodynamically meaningful, nor does it confirm the phase's thermodynamic stability. To accurately determine the transition temperature, we performed direct coexistence simulations[50] between the liquid and crystalline phases. At pressures where a plastic phase was found to emerge, we also simulated the coexistence between the plastic phase and the liquid at various temperatures, aiming to identify the point where the number of crystalline molecules fluctuates around 50%.

We defined a molecule as crystalline (either ice VII or plastic ice) evaluating Q_6, the rotational invariant first introduced by Steinhardt *et al.*[51] and optimized for different crystal phases by Lechner and Dellago.[52] Figure 2 shows the ice VII–liquid direct coexistence results for $P = 7$ GPa, suggesting that the coexistence temperature at this pressure is between 495 ±5 K. Similar results were obtained at all studied temperatures, providing a first estimate of the phase diagram.

At $P = 9$ GPa, direct coexistence simulations between the liquid and the plastic phase always evolved toward the liquid, indicating that the plastic phase is not thermodynamically stable at this pressure. Although the plastic phase could be generated by heating ice

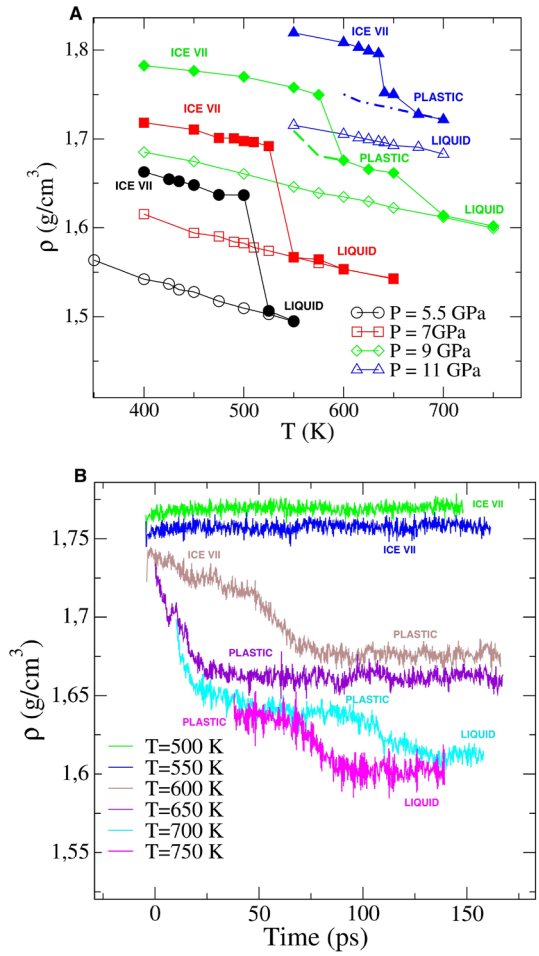

FIG. 1. (a) Temperature dependence of the density ρ for the four studied pressures. Filled symbols correspond to simulations initialized from a low-temperature Ice VII lattice and progressively equilibrated at higher temperatures. Open symbols represent simulations started from the liquid phase and cooled down to lower temperatures into metastable equilibrium. The green dashed line at $P = 9$ GPa shows a simulation initialized from the plastic phase and cooled to lower temperatures. The blue dot-dashed line at $P = 11$ GPa corresponds to a simulation initialized from the bulk liquid and cooled to lower temperatures. $P = 11$ GPa (blue) simulations do not extend above 700 K, as molecular dynamics runs at higher temperatures become numerically unstable. The error on the average densities was estimated with a block analysis to be smaller than the size of the symbols. (b) Time evolution of the density during NPT simulations at $P = 9$ GPa, starting from an Ice VII initial configuration. At low temperatures (blue and green lines), the Ice VII lattice is preserved. Upon increasing the temperature (brown and violet lines), the ice melts into the plastic phase. At higher temperatures (cyan, magenta, and orange lines), the plastic phase melts into the liquid. The simulation at $T = 750$ K appears shifted in time because it was initialized from a plastic configuration previously sampled at $T = 700$ K.

VII at 9 GPa, it remained metastable with respect to the liquid across all temperatures, i.e., more stable than ice VII, but not more stable than the liquid.

In contrast, at $P = 11$ GPa, we found clear evidence that the plastic phase is thermodynamically more stable than the liquid.

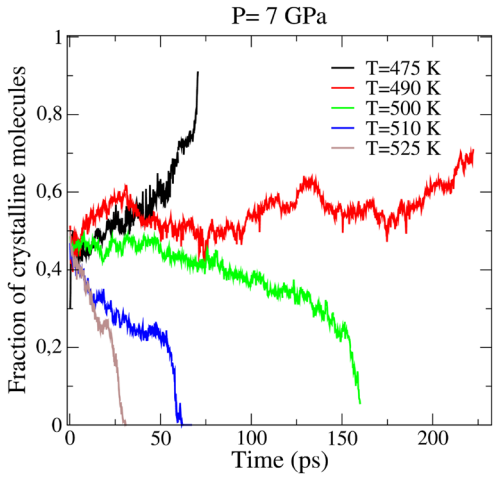

FIG. 2. Time evolution of the fraction of crystalline molecules in simulations initialized with half of the simulation box in the Ice VII lattice and the other half in the liquid phase, all performed at $P = 7$ GPa and various temperatures. The results show that, at low temperatures ($T \lesssim 450$ K), the crystalline region grows, while at higher temperatures ($T \gtrsim 450$ K), it melts, allowing us to bracket the coexistence temperature at this pressure.

Specifically, in direct-coexistence simulations between liquid water and ice VII at $T = 635$ K, the crystal transformed into a plastic phase, despite the lattice spacing being fixed in the orthogonal direction (see Fig. 3). At the same temperature, simulations of plastic–liquid coexistence showed that the plastic phase remained stable. Together, these observations demonstrated that, at this temperature, the plastic phase is the most stable among the three phases (ice VII, liquid, and plastic), confirming its thermodynamic stability at $P = 11$ GPa and $T = 635$ K.

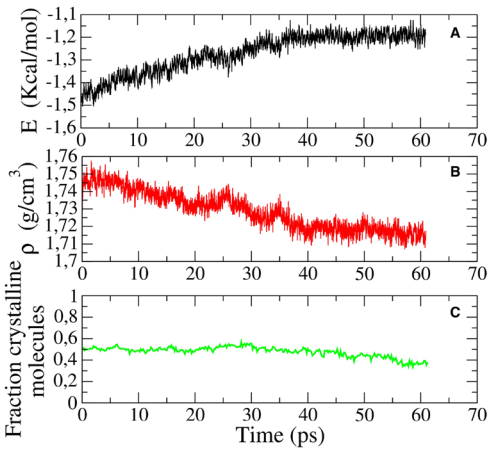

FIG. 3. Time evolution of the (a) potential energy, (b) density, and (c) fraction of crystalline molecules (as detected by Q_6) during a direct coexistence between liquid and crystal at $P = 11$ GPa and $T = 635$ K. Note that while the number of molecules in a crystalline environment remains similar, the density constantly decreases and the potential energy increases, signaling that Ice VII is turning into a plastic phase.

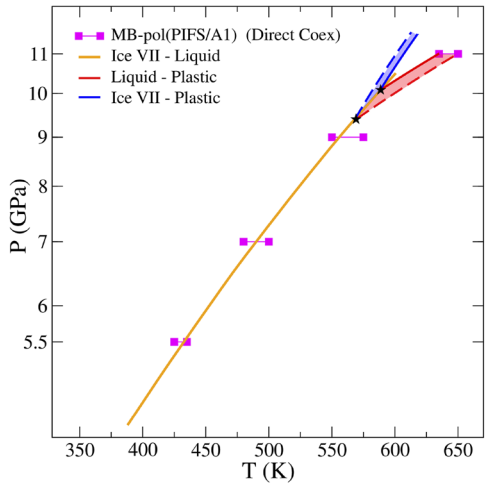

FIG. 4. Phase diagram of the MB-pol(PIFS/A1) model. Magenta symbols indicate the bracketing of the coexistence region obtained from direct coexistence simulations. At each pressure, the lower temperature point represents the highest temperature at which all trajectories of the Ice VII (or plastic) phase grow when in contact with the liquid, while the higher temperature point represents the lowest temperature at which the liquid phase grows in all trajectories where it is in contact with the Ice VII (or plastic) phase. The solid lines are the results of Gibbs–Duhem integration. Black stars mark the lower and upper bounds of the triple-point estimate, at T = 570 K, P = 9.4 GPa and T = 590 K, P = 10.1 GPa, respectively. Dashed regions represent the corresponding uncertainty ranges for the Ice VII–plastic and plastic–liquid coexistence lines above the triple point.

To accurately trace the coexistence lines, we employed Gibbs–Duhem thermodynamic integration (i.e., by numerically integrating the Clausius–Clapeyron equation), starting from the most reliable direct coexistence point at P = 7 GPa for the ice VII–liquid transition, as described in Ref. 44. Similarly, we determined the plastic–liquid coexistence curve, initiating the integration from a direct coexistence result at P = 11 GPa. These two coexistence curves, illustrated in Fig. 4, intersect at a point in the P–T plane. From this intersection, we initiated the Gibbs–Duhem integration[44] to map the coexistence boundary between plastic and ice VII. For this particular transition, direct coexistence methods are not applicable due to a mismatch in the lattice parameters of the two phases.

Figure 4 shows that the plastic phase emerges at pressures above the triple point, around P = 11 GPa, where all three phases (ice VII, plastic, and liquid) coexist. Beyond this point, the plastic phase occupies the region between ice VII and the liquid in the phase diagram. The resulting coexistence lines confirm the first-order character of both transitions and clearly delineate the stability region of the plastic phase at high pressure. Experimentally, the plastic phase is observed above P = 5 GPa.[27] The shift in pressure and temperature for the location of plastic ice is consistent with the shift in the ice VII melting line, with respect to the experimental measurement.[19]

B. Structural and dynamical differences between the phases

Having established the thermodynamic stability region of the VII plastic phase as predicted by the MB-pol(PIFS/A1) potential, we examined the structural and dynamic properties of the different phases.

Figure 5 shows the radial distribution functions $g(r)$, separated into components (OO, HH, OH). Ice VII shows well-defined peaks in all partial $g(r)$. The plastic phase retains weaker and less defined

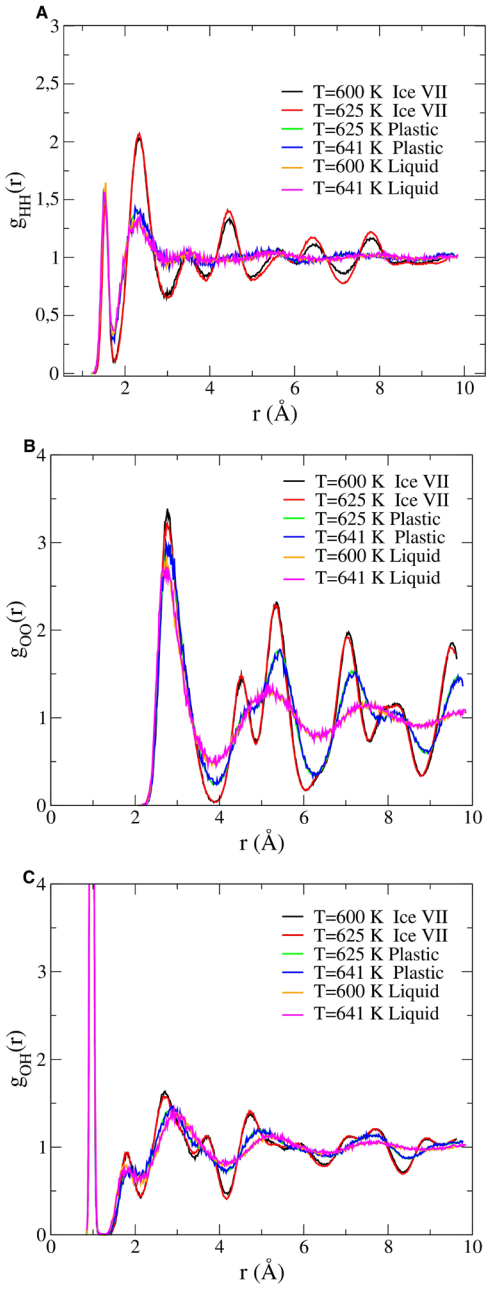

FIG. 5. Radial distribution functions at 11 GPa and different temperatures for (a) hydrogen–hydrogen, (b) oxygen–oxygen, and (c) oxygen–hydrogen atomic pairs. Thermodynamically stable and metastable states are shown when possible, to allow comparison between different phases at the same temperature.

correlations in $g_{OO}(r)$, signaling that the bcc lattice of the oxygen is distorted going from the ice VII to the plastic phase. In agreement with simulations using rigid water models,[16] very marked changes are seen in $g_{HH}(r)$, which is quite similar for both plastic ice and the liquid phase. Beyond the first peak of $g_{OH}(r)$, which reflects the intramolecular O–H bond, the oxygen–hydrogen radial distribution functions of the plastic and liquid phases closely resemble each other. This similarity highlights the substantial orientational and positional disorder of hydrogen atoms in the plastic phase.

The mean square displacement of oxygen atoms in the ice VII phase (on a bcc lattice) is primarily governed by vibrational motion around their equilibrium lattice positions. Similarly, the mean square displacement of the hydrogen atoms in ice VII is also expected to be governed by their vibrational motion. Interestingly, at 5.5 GPa, we observed a net diffusion of the H atoms, significantly larger than the vibrational component. This diffusion process, which must be connected to changes in the molecular orientation, being MB-pol(PIFS/A1) potential non-dissociable, indicates the presence of rotational jumps that rearrange the positions of the H atoms within the hydrogen-bond network. This rotational motion is not negligible even when the crystal is the thermodynamically stable phase. An analysis of the trajectories shows that these jump rotations take place around the C_2 axis of the molecules (the dipole vector direction). In this ~180° rotation, the two hydrogen atoms of the molecule swap their positions, preserving the oxygen–oxygen hydrogen-bond connectivity. These slow hydrogen motions were observed, within the time scale of our simulations, also at higher pressures. Figure 6 shows the mean square displacement for both hydrogen and oxygen atoms at $P = 7$ GPa for different temperatures in the stable ice VII phase. The data in Fig. 6 suggest that, with a switching timescale governed by temperature, the molecules undergo rotational motion and the hydrogen atoms switch their acceptor oxygens. Scaling along the time axis, the different mean-square displacements (Fig. S5) suggest that the slowing down of the dynamics is controlled by an Arrhenius process with an activation energy of about 12 000 K at this pressure.

Although ice VII can display rotational dynamics, this behavior is fundamentally different from that observed in the plastic phase. In ice VII, molecular reorientation is a thermally activated process that involves flipping the molecule around its dipole axis, thereby preserving the distinction between the two interpenetrating diamond sublattices. In contrast, in the plastic phase, orientational motion consists of rotational jumps that allow hydrogens to point toward oxygens belonging to both sublattices. Figure 7 shows the

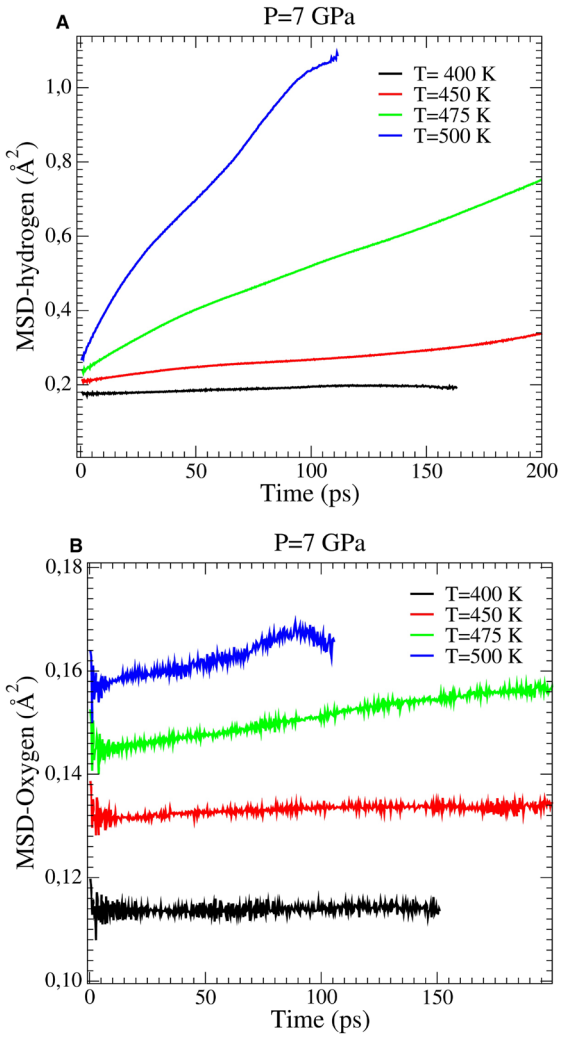

FIG. 6. Mean square displacement for (a) hydrogen and (b) oxygen atoms at 7 GPa and different temperatures in the Ice VII phase. Although the thermodynamically stable phase is Ice VII, the H atoms undergo a significant diffusional process, while the O atoms remain anchored around the lattice positions.

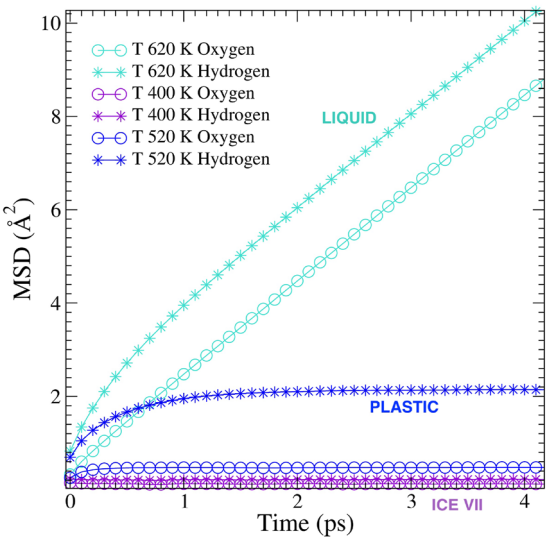

FIG. 7. Mean square displacement of oxygen (circles) and hydrogen (star) at $P = 8$ GPa. The three different phases (Ice VII, plastic ice, and liquid) are annotated and depicted in violet, blue, and turquoise, respectively. The dynamical behavior of plastic ice is signaled by a non-diffusive regime for oxygen (blue circles) and a diffusive regime for hydrogen (blue stars) on *ps* scale. In the Ice VII phase, both oxygen and hydrogen (violet circles and stars) do not diffuse. The linearity of liquid curves for both oxygen and hydrogen (turquoise circles and stars) indicates a diffusive regime on the *ps* timescale.

mean-square displacement (MSD) of oxygen and hydrogen atoms in the liquid, plastic, and ice VII phases. As expected, the dynamics in the liquid phase are fully diffusive. In both plastic and ice VII phases, the dynamics are instead caged, but the hydrogen MSD in the plastic phase reaches a much higher plateau, reflecting a larger mean-square vibrational amplitude (i.e., a higher Debye–Waller factor) associated with molecular rotations. As seen in the figure, the relaxation time of hydrogen reorientation in the plastic phase is on the sub-picosecond timescale, in good agreement with experimental observations and previous simulations.[27] To illustrate the difference in sublattice bonding, we compare the inherent structures of ice VII under two sets of conditions: one in which no molecular reorientations are observed on the simulation timescale (P = 7 GPa, T = 400 K), and one in which they are (P = 7 GPa, T = 475 K). This comparison is presented in Figs. 8(a) and 8(b), which show the probability distribution of the azimuthal angle between the hydrogen–oxygen bond vector and the [001] crystallographic direction. In a perfect bcc lattice, hydrogen atoms can orient along four equivalent diagonal directions within the [001] plane. In both panels, the red curves represent the angular distribution in the thermal (finite-temperature) simulations, showing broadened peaks around the four crystallographic directions, indicative of thermally activated reorientations. The black curves, obtained from energy-minimized configurations (i.e., inherent structures), reveal sharp peaks located precisely at the bcc orientations. In this way, all vibrational components are effectively suppressed, revealing the structure of the system at its local energy minimum. This analysis confirms that, despite thermal motion, the system remains confined to well-defined local minima corresponding to the ordered ice VII phase, i.e., no stable intermediate orientations emerge.

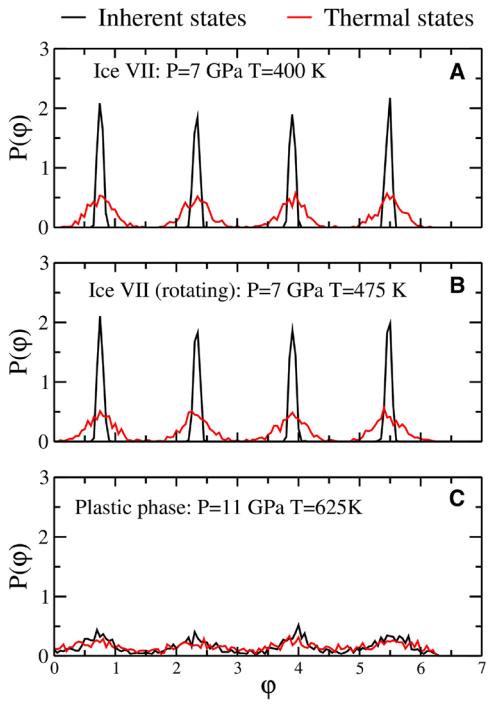

FIG. 8. Probability distribution of the azimuthal angle between hydrogen–oxygen distance and the [001] direction for (a) Ice VII at P = 7 GPa and T = 400 K, (b) Ice VII with high rotational diffusion at P = 7 GPa and T = 475 K, and (c) plastic phase at P = 11 GPa and T = 625 K. Red lines represent the probability distribution in the thermal state, while black lines in the inherent states, showing that Ice VII is the same state with and without rotational diffusion, differently from the plastic phase.

By contrast, Fig. 8(c) displays the same analysis for the plastic phase. Here, both the thermal and inherent state distributions exhibit a broad range of orientations, without sharp localization. This indicates that, in the plastic phase, orientational disorder is intrinsic and persists even after energy minimization. Furthermore, we find that the inherent structures include configurations in which the two interpenetrating sublattices of the bcc lattice become indistinguishable, namely, molecules can form hydrogen bonds with neighbors from both sublattices, highlighting the breakdown of the orientational order characteristic of ice VII.

IV. CONCLUSIONS

In summary, our simulations using the MB-pol (PIFS/A1) potential, an *ab initio* model parameterized on high-quality coupled cluster calculations, confirm the existence of the plastic phase recently observed experimentally. Direct coexistence simulations, and the observation of density hysteresis during heating ramps, demonstrate that the transition from ice VII to the plastic phase is first order, supporting earlier predictions from classical simulations[10–14] and resolving previous discrepancies with *ab initio* studies.[20,25] We find that the rotational dynamics of hydrogen atoms in the plastic phase occur on the picosecond timescale, in agreement with recent inelastic neutron scattering experiments. The analysis of inherent structure configurations further confirms that, as in the TIP4P/2005 model, hydrogen atoms in the plastic phase can transiently form bonds with both interpenetrating sublattices. In addition, we observe a much slower rotational process in ice VII, which effectively decorrelates hydrogen positions on the nanosecond timescale while consistently maintaining hydrogen bonding within the original sublattice.

At high densities and temperatures, the MB-pol (PIFS/A1) potential exhibits numerical instabilities. It remains unclear if this implies physical phenomena incompatible with the lack of explicit modeling of molecular dissociation or the presence of "holes" in the potential energy surface. We also note that MB-pol (PIFS/A1) locates the triple point between 9.4 and 10.1 GPa, with a significant deviation from the experimental estimate around 3.65 GPa. This discrepancy likely reflects limitations in the representation of the configurational space sampled at high pressure, in the treatment of higher-body interactions ($n > 3$), or in the neglect of nuclear quantum effects.

Further work is clearly required to understand the origin of the temperature and pressure discrepancies in the predicted location of the triple point. Such studies will ultimately enable a more accurate description of water at high pressures and contribute to unraveling the complex behavior of water under extreme conditions.

SUPPLEMENTARY MATERIAL

The supplementary material encompasses an error analysis for MB-pol (PIFS) potentials for ice VII, free energy differences between ice VII and ice VIII, and supplementary figures supporting the main text.

ACKNOWLEDGMENTS

F.G.M., J.R., and F.S. acknowledge the support from MIUR-PRIN 2022JWAF7Y, Cineca ISCRAB initiative, and ICSC-Centro Nazionale di Ricerca in High Performance Computing, Big Data and Quantum Computing, funded by the European Union "NextGenerationEU"). X.Z. and F.P. acknowledge the support from the Air Force Office of Scientific Research under Grant No. FA9550-20-1-0351, and allocations of computational resources from the Department of Defense High Performance Computing Modernization Program (HPCMP) and the Advanced Cyber infrastructure Coordination Ecosystem: Services and Support (ACCESS) program, which is supported by the National Science Foundation (Grant Nos. 2138259, 2138286, 2138307, 2137603, and 2138296). L.E.B. acknowledges the financial support by the European Union - NextGenerationEU (PRIN N. 2022NRBLPT), the ANR-23-CE30-0034 EXOTIC-ICE, and the Swiss National Fund (FNS) under Grant No. 212889. We dedicate this article to Carlos Vega for his enduring contributions to the physics of liquids, particularly water.

AUTHOR DECLARATIONS

Conflict of Interest

The authors have no conflicts to disclose.

Author Contributions

Francesco Guidarelli Mattioli: Conceptualization (equal); Data curation (equal); Formal analysis (equal); Investigation (equal). **Xuanyu Zhu**: Conceptualization (equal); Data curation (equal); Formal analysis (equal); Investigation (equal). **Francesco Paesani**: Conceptualization (equal); Data curation (equal); Formal analysis (equal); Investigation (equal). **Livia E. Bove**: Conceptualization (equal); Data curation (equal); Formal analysis (equal); Investigation (equal). **John Russo**: Conceptualization (equal); Data curation (equal); Formal analysis (equal); Investigation (equal). **Francesco Sciortino**: Conceptualization (equal); Data curation (equal); Formal analysis (equal); Investigation (equal).

DATA AVAILABILITY

The data that support the findings of this study are available within the article. The public domain LAMMPS code has been used to generate the trajectories for all different state points. Code for the Gibbs–Duhem integration, input file and representative trajectory have been provided on Zenodo at https://doi.org/10.5281/zenodo.17350531.

REFERENCES

[1] J. L. Finney, *Water: A Very Short Introduction* (Oxford University Press, 2015), Vol. 440.
[2] P. Gallo, K. Amann-Winkel, C. A. Angell, M. A. Anisimov, F. Caupin, C. Chakravarty, E. Lascaris, T. Loerting, A. Z. Panagiotopoulos, J. Russo *et al.*, Chem. Rev. **116**, 7463 (2016).
[3] C. G. Salzmann, J. Chem. Phys. **150**, 060901 (2019).
[4] B. Kamb and B. L. Davis, Proc. Natl. Acad. Sci. U. S. A. **52**, 1433 (1964).
[5] B. Journaux, K. Kalousová, C. Sotin, G. Tobie, S. Vance, J. Saur, O. Bollengier, L. Noack, T. Rückriemen-Bez, T. van Hoolst *et al.*, Space Sci. Rev. **216**, 1 (2020).
[6] M. Lingam and A. Loeb, Rev. Mod. Phys. **91**, 021002 (2019).
[7] M. C. Nixon and N. Madhusudhan, Mon. Not. R. Astron. Soc. **505**, 3414 (2021).
[8] T. Van Hoolst, G. Tobie, C. Vallat, N. Altobelli, L. Bruzzone, H. Cao, D. Dirkx, A. Genova, H. Hussmann, L. Iess, J. Kimura, K. Khurana, A. Lucchetti, G. Mitri, W. Moore, J. Saur, A. Stark, A. Vorburger, M. Wieczorek, A. Aboudan, J. Bergman, F. Bovolo, D. Breuer, P. Cappuccio, L. Carrer, B. Cecconi, G. Choblet, F. De Marchi, M. Fayolle, A. Fienga, Y. Futaana, E. Hauber, W. Kofman, A. Kumamoto, V. Lainey, P. Molyneux, O. Mousis, J. Plaut, W. Puccio, K. Retherford, L. Roth, B. Seignovert, G. Steinbrügge, S. Thakur, P. Tortora, F. Tosi, M. Zannoni, S. Barabash, M. Dougherty, R. Gladstone, L. I. Gurvits, P. Hartogh, P. Palumbo, F. Poulet, J.-E. Wahlund, O. Grasset, and O. Witasse, Space Sci. Rev. **220**, 54 (2024).
[9] M. Matsumoto, T. Yagasaki, and H. Tanaka, J. Chem. Phys. **160**, 094101 (2024).
[10] Y. Takii, K. Koga, and H. Tanaka, J. Chem. Phys. **128**, 204501 (2008).
[11] K. Himoto, M. Matsumoto, and H. Tanaka, Phys. Chem. Chem. Phys. **13**, 19876 (2011).
[12] K. Himoto, M. Matsumoto, and H. Tanaka, J. Phys. Soc. Jpn. **81**, SA023 (2012).
[13] J. L. Aragones, M. M. Conde, E. G. Noya, and C. Vega, Phys. Chem. Chem. Phys. **11**, 543 (2009).
[14] J. L. Aragones and C. Vega, J. Chem. Phys. **130**, 244504 (2009).
[15] A. Toffano, J. Russo, M. Rescigno, U. Ranieri, L. E. Bove, and F. Martelli, J. Chem. Phys. **157**, 094502 (2022).
[16] A. Henao, J. M. Salazar-Rios, E. Guardia, and L. C. Pardo, J. Chem. Phys. **154**, 104501 (2021).
[17] I. Skarmoutsos, S. Mossa, and E. Guardia, J. Chem. Phys. **150**, 124506 (2019).
[18] J.-A. Hernandez and R. Caracas, J. Chem. Phys. **148**, 214501 (2018).
[19] Y. Adachi and K. Koga, J. Chem. Phys. **153**, 114501 (2020).
[20] L. Zhang, H. Wang, R. Car, and W. E, Phys. Rev. Lett. **126**, 236001 (2021).
[21] H. Wang, L. Zhang, J. Han, and W. E, Comput. Phys. Commun. **228**, 178 (2018).
[22] J. Sun, A. Ruzsinszky, and J. P. Perdew, Phys. Rev. Lett. **115**, 036402 (2015).
[23] K. Sharkas, K. Wagle, B. Santra, S. Akter, R. R. Zope, T. Baruah, K. A. Jackson, J. P. Perdew, and J. E. Peralta, Proc. Natl. Acad. Sci. U. S. A. **117**, 11283 (2020).
[24] S. Dasgupta, E. Lambros, J. P. Perdew, and F. Paesani, Nat. Commun. **12**, 6359 (2021).
[25] A. Reinhardt, M. Bethkenhagen, F. Coppari, M. Millot, S. Hamel, and B. Cheng, Nat. Commun. **13**, 4707 (2022).
[26] R. Yamane, K. Komatsu, and H. Kagi, Phys. Rev. B **104**, 214304 (2021).
[27] M. Rescigno, A. Toffano, U. Ranieri, L. Andriambariarijaona, R. Gaal, S. Klotz, M. M. Koza, J. Ollivier, F. Martelli, J. Russo *et al.*, Nature **640**, 662 (2025).
[28] S. Klotz, Th. Strässle, and L. E. Bove, Appl. Phys. Lett. **103**, 193504 (2013).
[29] S. K. Reddy, S. C. Straight, P. Bajaj, C. Huy Pham, M. Riera, D. R. Moberg, M. A. Morales, C. Knight, A. W. Götz, and F. Paesani, J. Chem. Phys. **145**, 194504 (2016).
[30] E. Palos, E. F. Bull-Vulpe, X. Zhu, H. Agnew, S. Gupta, S. Saha, and F. Paesani, J. Chem. Theory Comput. **20**, 9269 (2024).
[31] S. L. Bore and F. Paesani, Nat. Commun. **14**, 3349 (2023).
[32] F. Sciortino, Y. Zhai, S. L. Bore, and F. Paesani, Nat. Phys. **21**, 480 (2025).
[33] O. Mishima and T. Sumita, J. Phys. Chem. B **127**, 1414 (2023).
[34] V. Babin, C. Leforestier, and F. Paesani, J. Chem. Theory Comput. **9**, 5395 (2013).
[35] V. Babin, G. R. Medders, and F. Paesani, J. Chem. Theory Comput. **10**, 1599 (2014).
[36] G. R. Medders, V. Babin, and F. Paesani, J. Chem. Theory Comput. **10**, 2906 (2014).
[37] W. L. Jorgensen, J. Chandrasekhar, J. D. Madura, R. W. Impey, and M. L. Klein, J. Chem. Phys. **79**, 926 (1983).
[38] J. L. F. Abascal and C. Vega, J. Chem. Phys. **123**, 234505 (2005).
[39] X. Zhu and F. Paesani, J. Chem. Theory Comput. **21**, 6950–6963 (2025).
[40] A. P. Thompson, H. M. Aktulga, R. Berger, D. S. Bolintineanu, W. M. Brown, P. S. Crozier, P. J. in't Veld, A. Kohlmeyer, S. G. Moore, T. D. Nguyen *et al.*, Comput. Phys. Commun. **271**, 108171 (2022).
[41] M. Riera, C. Knight, E. F. Bull-Vulpe, X. Zhu, H. Agnew, D. G. A. Smith, A. C. Simmonett, and F. Paesani, J. Chem. Phys. **159**, 054802 (2023).

[42]S. Gupta, E. F. Bull-Vulpe, H. Agnew, S. Iyer, X. Zhu, R. Zhou, C. Knight, and F. Paesani, J. Chem. Theory Comput. **21**, 1838–1849 (2025).
[43]J. Russo, F. Romano, and H. Tanaka, Nat. Mater. **13**, 733 (2014).
[44]D. A. Kofke, J. Chem. Phys. **98**, 4149 (1993).
[45]C. Pérez, M. T. Muckle, D. P. Zaleski, N. A. Seifert, B. Temelso, G. C. Shields, Z. Kisiel, and B. H. Pate, Science **336**, 897 (2012).
[46]Y. Wang, V. Babin, J. M. Bowman, and F. Paesani, J. Am. Chem. Soc. **134**, 11116 (2012).
[47]V. Babin and F. Paesani, Chem. Phys. Lett. **580**, 1 (2013).
[48]L. Evangelisti, C. Perez, S. Lobsiger, N. A. Seifert, D. P. Zaleski, B. Pate, Z. Kisiel, B. Temelso, and G. C. Shields, in *69th International Symposium on Molecular Spectroscopy* (ISMS, 2014), p. FD12.
[49]S. E. Brown, A. W. Götz, X. Cheng, R. P. Steele, V. A. Mandelshtam, and F. Paesani, J. Am. Chem. Soc. **139**, 7082 (2017).
[50]M. M. Conde, M. Rovere, and P. Gallo, J. Chem. Phys. **147**, 244506 (2017).
[51]P. J. Steinhardt, D. R. Nelson, and M. Ronchetti, Phys. Rev. B **28**, 784 (1983).
[52]W. Lechner and C. Dellago, J. Chem. Phys. **129**, 114707 (2008).